Jour. Fac. Sci., Hokkaido Univ., Ser. VII (Geophysics), Vol. 8, No. 2, 137-153, 1987.

Vortex Generation by Multiple Source-Sink Forcing in a Rotating Tank

Momoki Koga and Sei-ichi Kanari

Department of Geophysics, Faculty of Science, Hokkaido University, Sapporo 060, Japan.

(Received November 10, 1986)

Abstract

This study investigates the fundamental features of a vortex field generated by multiple source-sink forcing in a rotating system. The experiment was conducted using a cylindrical tank (38 cm in diameter, 52 cm in depth) containing homogeneous fluid and covered with a transparent horizontal plate to eliminate β-effect. A turbulent fluid was produced with multiple source-sink flows at the bottom of the tank. The instantaneous flow pattern (velocity distribution) was measured photographically by a flow visualization technique using small neutrally buoyant beads (1.1 mm in diameter) as tracers, at three different rates of tank rotation (0.43, 0.81, 1.15 rad/s). The detailed spatial distribution of velocity and vorticity in the upper part of the tank shows that the flow fields are nearly two dimensional and geostrophic with many distinctive horizontal vortices. The number of the vortices increases with the rotation rate, but the ratio of clockwise vortices to the total number of vortices remains fairly constant at about 0.7. The spatial mean of the vorticity (vertical component) also remains constant, close to zero (less than about 6% of the standard deviation of the vorticity distribution) at any rotation rate, in spite of the increase in absolute velocity and vorticity that accompanies any increase in the rotation rate. These facts indicate some dynamical similarity, which holds at any rotation rate, in the generation of vortices (redistribution of vorticity) as an effect of rotation. Supplementary experimental results with a single source or sink forcing at the bottom are also discussed in comparison with the above multiple source-sink forcing experiments.

1. Introduction

Previous laboratory experiments have described the generation processes of vortices in a rotating system including interaction processes between the generated vortices. Early works by Long (1956, 1958) and more detailed experiments by Shih & Pao (1971) showed that a weak source or sink on an axis of rotation led to generation of a vortex along its axis. This sort of single vortex has also been generated in studies of tornado vortices. Turner & Lilly (1962) showed

that ascending bubbles created a vortex field in their axial forcing flow, and Morton (1983) generated a vortex field by injecting buoyant fluid along an axis. MacEwan (1976) demonstrated that a field of vortices can be generated by multiple source and sink jets at the bottom of a tank. The intense vortices generated were nearly two-dimensional and slowly drifted, independent of their position relative to the jets within the tank, through mutual interaction. He discussed the generation process of vortices from the point of view of the vorticity expulsion hypothesis, according to which vorticity comes from the redistribution of angular momentum by a turbulent convective process within a fluid undergoing initially uniform rotation (e.g. Gough & Lynden-bell (1968), Bretherton & Turner (1968), Tritton (1978)). Colin de Verdiere (1980) focused on the interaction process, such as the coalescence of two-dimensional vortices which were generated by bottom sources and sinks slowly oscillating in time on a f-plane and a β-plane. He observed that the energy containing scale is significantly larger than the forcing scale.

Vortices can be also excited by an oscillating grid at the bottom or the top of a tank as seen in experiments by Hopfinger *et al.* (1982) and Dickinson & Long (1983). These studies focused on the transition phenomena from strongly three-dimensional turbulence near the oscillating grid to a nearly two-dimensional turbulent flow of vortices dominated by rotation. Hopfinger *et al.* (1982) also investigated the population of vortices and the behavior of the concentrated vortex core in two-dimensional vortices.

The above experiments demonstrated the generation processes of nearly two-dimensional vortices in a rotating system using various methods of forcing. The generation and interaction processes were discussed from the point of view of the redistribution process of vorticity based on the measurements of mean velocity and vorticity. However, information was still lacking on the detailed spatial distribution of vortices, including the change in their distribution over time. In order to examine the redistribution process of vorticity more clearly, we found it necessary to measure the instantaneous spatial distribution of vorticity in vortex fields.

The present experiment uses a deep tank with multiple source-sink forcing at the bottom to generate vortices. We focus on the velocity field in the upper part of the tank where nearly two-dimensional vortices dominated by tank rotation are seen. Using a flow visualization technique, instantaneous detailed spatial distributions of velocity are measured in a horizontal section of the upper part of the tank. Based on the measured velocity destributions, spatial distributions of vorticity are estimated. These are useful for examining the redistribu-

tion process of vorticity. We can also examine change in the vortex field with a sequential flow visualization. Supplementary experiments with a single source or sink forcing at the bottom are also conducted in order to examine the fundamental characteristics of the flow field with the single forcing in the present tank system.

2. Experiment

2.1 Experimental apparatus

The experiment was conducted in a transparent cylindrical tank made of acrylate resin, 38 cm in diameter and 52 cm in depth, shown schematically in Fig. 1 (a). The tank was filled with a homogeneous fluid and the forcing of the fluid was effected by the source and sink flows at the bottom of the tank. The

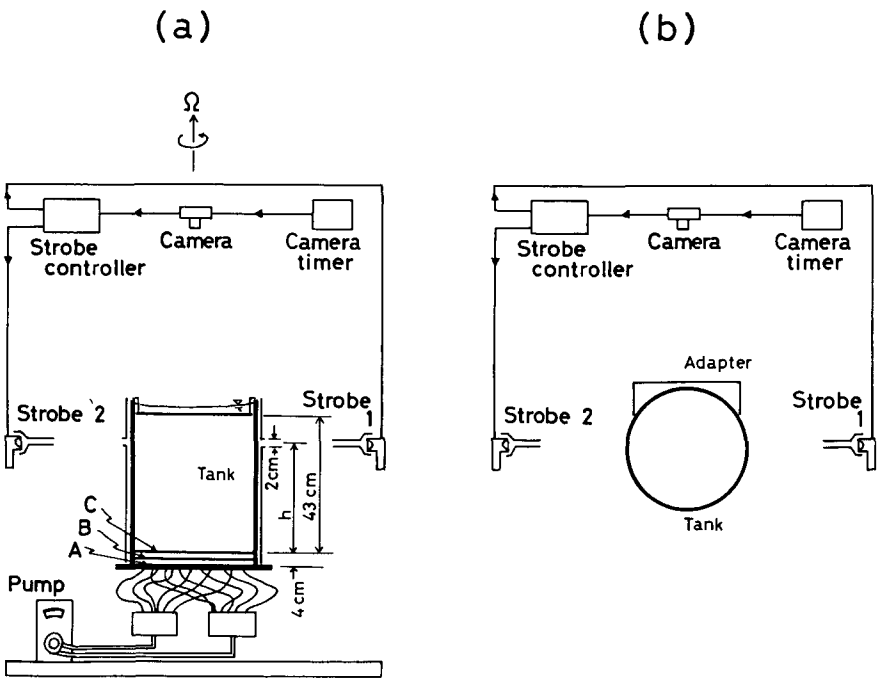

Fig. 1 Schematic picture of the experimental set-up. Both the tank system and the camera system (excluding the timer) are mounted on the turntable. (a) Side view of the tank system with the camera system for flow visualization of the horizontal section of the tank. (b) Overhead view with the camera system for flow visualization of the vertical section. Photographs are taken through a optical adapter to eliminate the horizontal distortion of the picture.

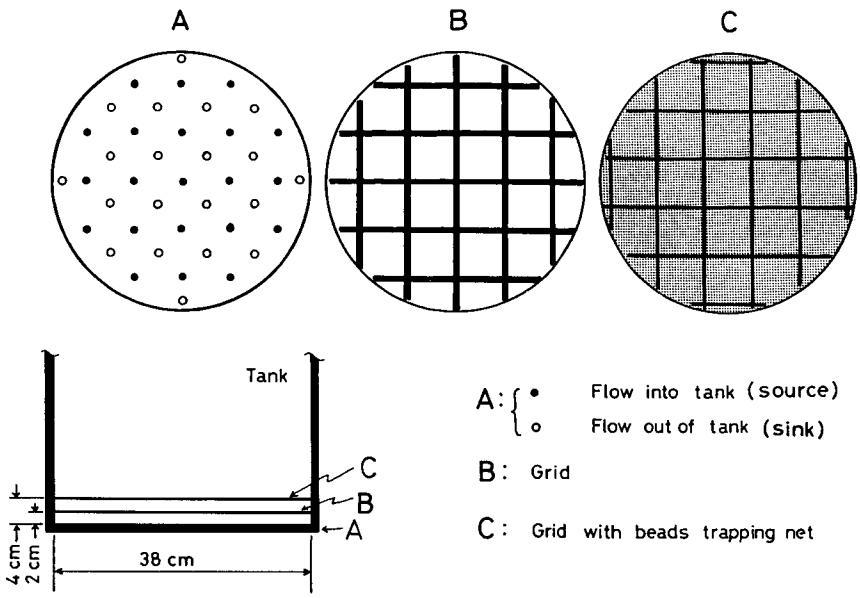

Fig. 2 Arrangement of source and sink holes at the tank bottom (**A**). The diameter of each hole is 4 mm. Grids **B** and **C** are for diffusing the source and sink flows.

arrangement of the source and sink flows and the two grids which are used for diffusing the flows, are shown in Fig. 2. A transparent plane cover was placed just beneath the free surface to eliminate β-effects. Both the tank and a camera system for flow visualization were mounted on a 120 cm diameter turntable whose rotation rate can be adjusted continuously up to 15 r.p.m (counterclockwise direction).

2.2 Flow visualization technique

The flow patterns and the velocity distribution in the cylindrical tank were measured photographically with a flow visualization technique using small neutrally buoyant polystyren beads (1.1 mm in diameter, 1.08 in specific gravity) as tracers. The density of the homogeneous fluid (salt water) in the tank was adjusted to make to beads neutrally buoyant.

The flow field in the horizontal section of the tank was measured by the camera system, shown in Fig. 1 (a). Strobes flash through a horizontal slit 2 cm thick and photographs were taken from above by a 35-mm still camera. The flow field in the vertical section was measured by the system in Fig. 1 (b). Photographs were taken from the side through an optical adapter (the space

between the transparent vertical plate and the cylindrical wall of the tank was filled with water). This adapter reduces the horizontal distortion of the picture to less than 1%.

The movement of the tracer beads was measured photographically with an overlapping photographing technique developed by Koga (1981). This technique uses multiple strobes, flashing one after another at short intervals through optical filters of different colors. Using this technique, images of beads at different instants are photographed in a single exposure, from which temporal relationship between the overlapping exposed images can easily be determined by their color sequence. In the present experiment, two color strobes, Strobe 1 (red) and Strobe 2 (blue), were used as shown in Fig. 1. The required time interval and the number of strobe flashes per exposure were controlled by a strobe controller (a quartz-synchronized programmable signal retarder) which was specially designed for the present experiment. We can select any time interval and number of flashes using the retarder. In the present study, we used one flash of red followed by 3 flashes of blue at intervals of one second or so per exposure.

The photographs were analyzed in the following way. Each of 35-mm negatives was projected onto a large sheet of paper, and the positions of photographed beads were traced on the paper. Each pair of traced positions (the position of each bead both at the first flash and the last flash) was read by a digitizer to make digitized co-ordinate data for computer data processing. We were able to calculate the spatial distribution of velocity using these data. Velocities in typical vortices in the present experiment ranged from 0.1 cm/s to 0.3 cm/s. The estimated degree of error in the above analysis was within ± 0.01 cm/s.

2.3 Experimental procedure

This study focuses mainly on the flow field in a horizontal section of the upper part of the tank where the flow is nearly horizontal due to the effect of tank rotation. Most of the measurements were conducted in one horizontal section of the upper part of the tank at three different tank rotation rates with constant fluid forcing at the tank bottom, as shown in Table 1.

Supplementary experiments with a single source or sink flow at the bottom of the tank (Fig. 3 (a), (b)) were also conducted. They show a characteristic flow structure generated by the single source or sink forcing in the present tank system. They also reveal the difference between the multiple-forced flow fields and the single-forced ones. The flow from the single source or sink in the

Table 1 Laboratory parameter values Ω, Q and the achieved velocity field and parmeters in the upper part of the tank.

	Case I	Case II	Case III
Tank rotation Ω(rad/s)	0.43	0.81	1.15
Pump flow rate Q(cm^3/s)	22.1	22.1	22.1
Mean velocity U(cm/s)	0.11	0.12	0.15
Vortex scale L(cm)	10.2	8.1	7.5
Rossby number $R_0 = U/2\Omega L$	1.3×10^{-2}	9.1×10^{-3}	8.7×10^{-3}
Reynolds number $R_e = UL/\nu$	102	88	102

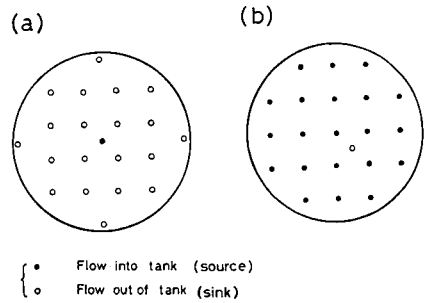

Fig. 3 Arrangement of source and sink holes in the supplementary experiments. (a) Single source forcing. (b) Single sink forcing. The remaining sinks of (a) and sources of (b) are for conserving the water mass in the tank. Flows from these are relatively weak.

supplementary experiment was adjusted to equal the flow from each source or sink in the multiple source-sink forcing experiment. The remaining sinks for the single source experiment and the remaining sources for the single sink experiment in the Fig. 3 (a), (b) are for conserving water mass in the tank. Therefore, the flow from each of these remaining sinks or sources is much weaker than the forcing flow.

3. Experimental results

3.1 Flow field by the visualization

An example of the flow visualization in the vertical section is shown in Fig. 4 (a) at a rotation rate Ω of 0.81 rad/s. The flow field in the lower part of the tank is three dimensional and that in the upper part is nearly two dimensional,

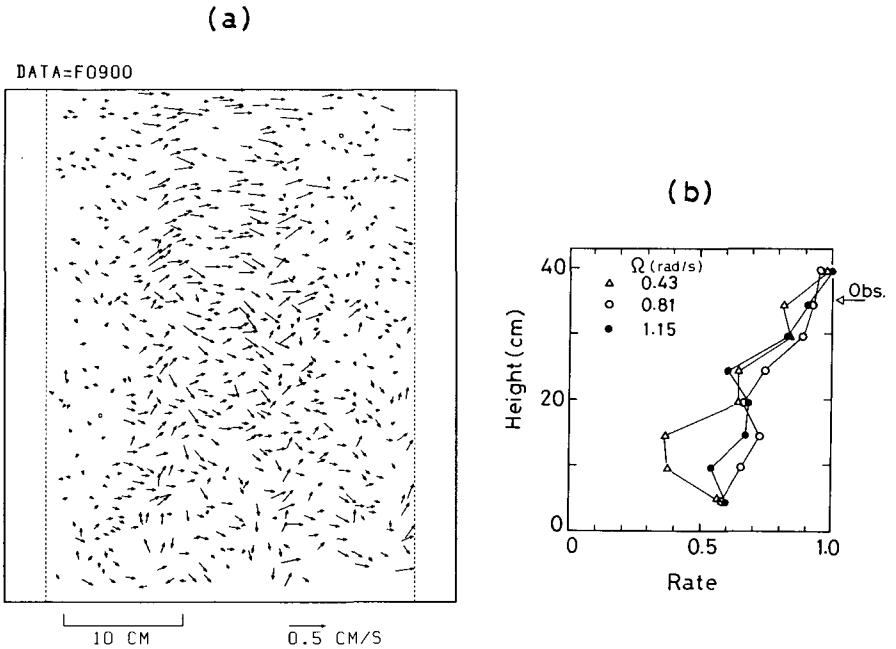

Fig. 4 Flow field in the vertical section of the tank. (a) An example of the visualized flow field in a rotational frame at rotation rate $\Omega=0.81$ rad/s. Each vector shows the velocity vector measured by the movement of a tracer bead. The visualized area extends from the bottom (grid **C**) to the upper horizontal plate, enclosed by two dotted lines. (b) Rate of the velocity vectors whose directions are within 45 degrees from horizontal as a function of height. The arrow marks the position of the visualization in the horizontal section ($h=35.5$ cm).

and shows distinctive horizontal velocity vectors. Figure 4 (b) shows the rate of the velocity vectors whose directions are within 45 degrees from horizontal as a function of height for the data of Fig. 4 (a), alongside two other cases at different rotation rates. Though the difference between the three distributions is not marked, more than 80% of vectors are within 45 degrees from horizontal at heights higher than 30 cm at any rotation rate. In the following, visualizations in the horizontal section are conducted at a height h of 35.5 cm above the bottom grid, where the distinctive horizontal movement is seen.

In Fig. 5 (a), an example of the instantaneous velocity field in the horizontal section is shown for $\Omega=0.81$ rad/s. We can see intense vortices generated by the effect of rotation. Interporated velocity distribution on the 1×1 cm grid points is also shown in Fig. 5 (b). The interporation at each grid point is made through the second derivatives using neighbour velocity data (two dimensional

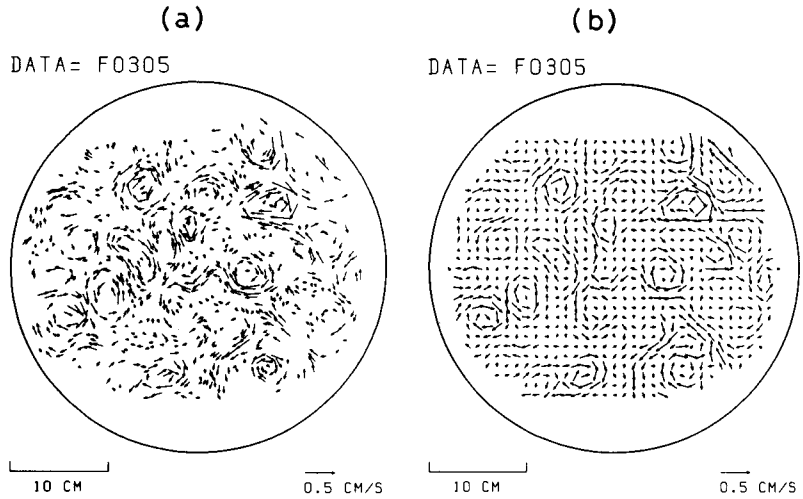

Fig. 5 (a) An Example of the visualized velocity field in the horizontal section ($h=$ 35.5 cm) at $\Omega=0.81$ rad/s. (b) The interporated distribution.

C^2 interporatation scheme for irregulary spaced data). Though the interporated velocity distribution may be somewhat smooth compared to the original, interporated regulary spaced data are suitable for estimating relative frequencies of the velocity distribution and the vorticity distribution.

Both the Coriolis force $2\Omega v$ and the centrifugal force v^2/r relative to each of the vortex centers are estimated using the visualized detailed velocity distribution, where v is the azimuthal velocity and r the distance from the vortex center. Figure 6 (a) and 6 (b) show examples of the estimated forces of clockwise and counterclockwise vortices seen in Fig. 5 (a). The scales of the vortices average about 3 cm in diameter where the azimuthal velocity attains maximum velocity and 8 cm where the velocity approaches zero. The force estimates show that the magnitude of the centrifugal force is no more than 8% of that of the Coriolis force at any rotation rate. This indicates that the flow field is nearly in geostrophic balance.

3.2 Population of vortices and change in vortex population over time

Center positions of the distinctive vortices in the horizontal section were read from negative films which were taken at intervals of 30 s. The distributions of these center positions and their corresponding time are shown in Fig. 7 (a), (b), (c) at three different rotation rates. The open circles and the open squares indicate clockwise (opposite direction to tank rotation) vortices and

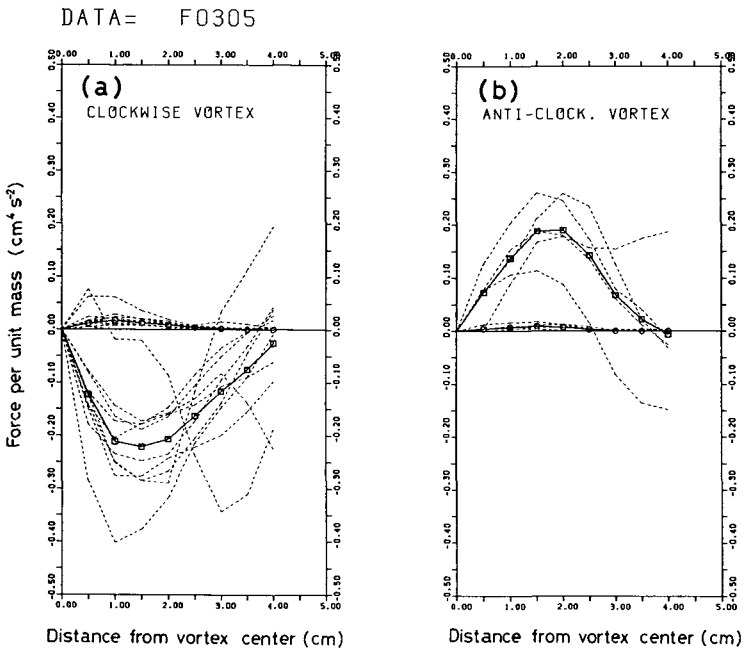

Fig. 6 Distributions of Coriolis force and centrifugal force relative to each vortex center (dashed lines) in a rotational frame, for the data Fig. 5 (a). Mean distributions are shown by solid lines with squares (Coriolis force) and circles (centrifugal force).

counterclockwise vortices, respectively. The number on the upper right side of each circle or square mark shows the frame number of the negative film. Hence, we can trace the change of the vortex field over time by following these numbers. Some vortices merge occasionally, but it seems that others form spontaneously, keeping the population constant. These figures show that the position of the vortex becomes more unstable and the life time of the vortex becomes shorter as the rotation rate is decreased.

Figure 8 (a) shows both the total nuumber (population) of the vortices and the rate of clockwise vortices relative to the total as a function of time, estimated using the succeeding 12 frames. Figure 8 (b) shows the mean population and the mean rate as a function of the rotation rate of the tank. The population increases as the rotation rate increases, but the rate of clockwise vortices relative to the total is nearly the same, about 0.7, at any rotation rate.

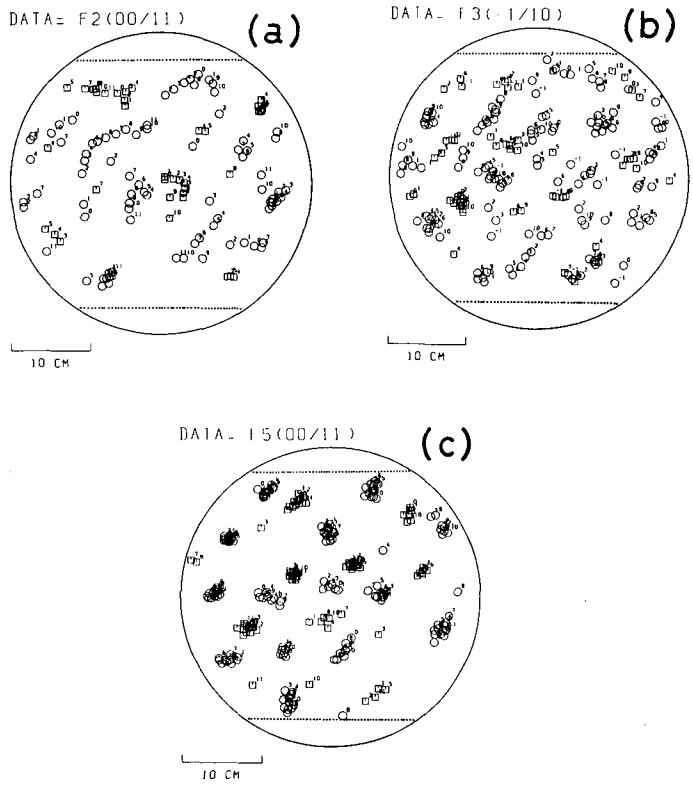

Fig. 7 Distributions of center positions of the distinctive vortices and their time change. The distributions from 12 frames taken at interval of 30 s are superimposed. Two dotted lines indicate the margins of the visualized area. An open circle and an open square indicate clockwise and counterclockwise vortices, respectively. The number on the upper right side of each mark shows the frame number of the film. (a) $\Omega=0.43$ rad/s, (b) $\Omega=0.81$ rad/s, (c) $\Omega=1.15$ rad/s.

3.3 Frequency distributions of velocity and vorticity

The frequency distribution in the absolute value of velocity is estimated using the interporated velocity data from within 15 cm of the center in the horizontal section of the tank. The distributions at three different rotation rates (0.43, 0.81, 1.15 rad/s) are shown in Fig. 9 (a). The distribution at each rotation rate is a mean of the three independent instantaneous velocity distributions interporated as shown in Fig. 5 (b). Most of the absolute values range from 0.1 to 0.15 cm/s and the values increase a little with the rotation rate.

The vorticity (vertical component) at each grid point is calculated using the

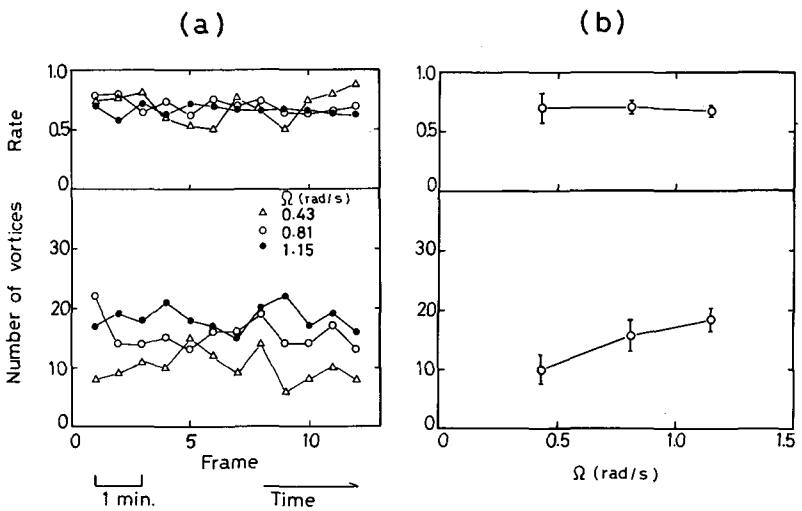

Fig. 8 (a) Total number of distinctive vortices and rate of clockwise vortices as a function of time. (b) Mean total number and rate as a function of tank rotation. Vertical bars indicate the standard deviations.

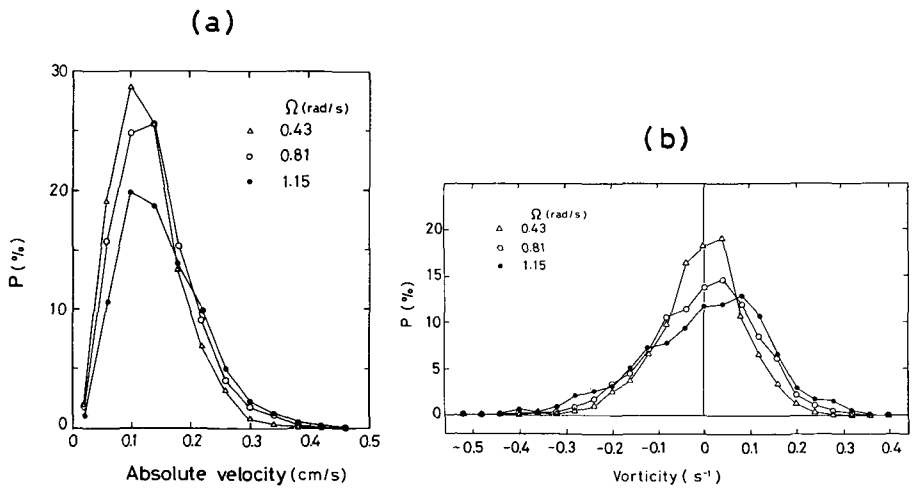

Fig. 9 (a) Frequency distributions of absolute value of velocity. (b) Frequency distributions of vorticity (vertical component).

four interporated velocity values near the grid point. Figures 10 (a), (b) and (c) show examples of the calculated distribution of vorticity. The frequency distribution of vorticity is also estimated, using the calculated vorticity values within a range of 15 cm from the center. The distributions at three different

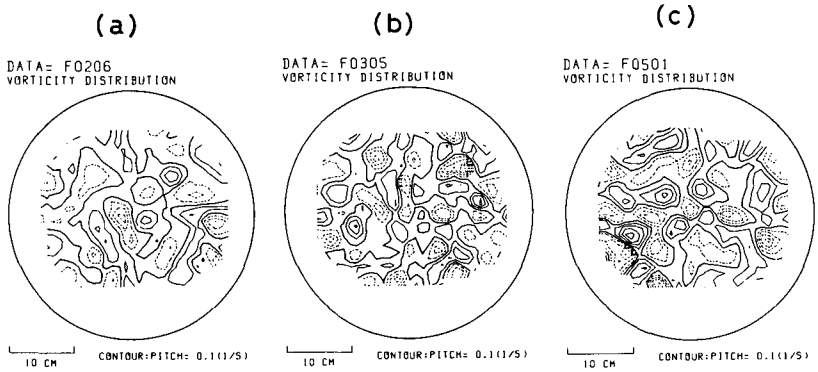

Fig. 10 Examples of the distribution of vorticity in the horizontal section (h=35.5 cm). (a) $\Omega=0.43$ rad/s, (b) $\Omega=0.81$ rad/s, (c) $\Omega=1.15$ rad/s. Thin solid contour lines and dashed contour lines indicate positive and negative vorticity contours respectively.

rotation rates are shown in Fig. 9 (b). As with the measurements of velocity distribution, these are also means of three independent measurements. They are nonsymmetrical, extend further on the negative side, and become broader as the rate of rotation is increased. This nonsymmetrical frequency distribution would be consistant with the predominance of clockwise vortices. Mean standard deviations are 0.093, 0.116 and 0.137 1/s for the rotation rates 0.43, 0.81 and 1.15 rad/s, respectively. These are relatively small values, between 6% and 10% of 2Ω, the background vorticity due to tank rotation. In spite of the broader distribution as the rotation rate increases, the total mean of the vorticity in each distribution is nearly zero at any rotation rate (almost less than 6% of the standard deviation). The skewness of the distribution has no clear dependency on the rotation rate, having nearly the same mean value of -0.4 at any rotation rate. The mean value, the standard deviation and the skewness of the distribution in each measurement are summarized in Table 2.

3.4 Results of supplementary experiments

Flow fields in the horizontal section forced by a single source are shown in Fig. 11 (a), (b), (c) at three different rotation rates of the tank, 0.43, 0.81 and 1.15 rad/s, respectively. A single distinctive clockwise (high-pressure) vortex is seen in the center of the section, over the position of forcing. The souce forcing compresses a water column just over it, increasing the negative relative vorticity (a clockwise vortex). The scale of the vortex decreases as the rotation rate is increased. The flow field is nearly geostrophic, where the magnitude of

Table 2 Measured velocity and vorticity distributions.

	Ω (rad/s)	Data	Velocity distribution			Velocity distribution		
			Mean velocity (cm/s)	Standard deviation (cm/s)	Skewness	Mean velocity (1/s)	Standard deviation (1/s)	Skewness
Case I	0.43	F 0206	0.117	0.058	0.68	−0.006	0.100	−0.11
		F 0211	0.106	0.055	1.10	−0.005	0.088	−0.30
		F 0216	0.102	0.058	1.23	−0.007	0.090	−0.89
		Mean	0.108	0.057	1.00	−0.006	0.093	−0.43
Case II	0.81	F 0105	0.123	0.068	0.90	0.003	0.111	−0.62
		F 0305	0.123	0.062	0.81	−0.005	0.124	−0.32
		F 0309	0.115	0.062	0.94	−0.004	0.114	−0.22
		Mean	0.120	0.064	0.88	−0.002	0.116	−0.39
Case III	1.15	F 0111	0.141	0.078	0.82	0.005	0.126	−0.80
		F 0501	0.159	0.080	0.63	0.002	0.144	−0.24
		F 0507	0.149	0.079	0.65	0.001	0.141	−0.31
		Mean	0.150	0.079	0.70	0.003	0.137	−0.45

the centrifugal force is no more than 6% of that of the Coriolis force, as was the case in the previous multi-forcing experiments.

Figure 11 (d) shows the flow field forced by a single sink at the rotation rate of 0.81 rad/s. A weak counterclockwise (low-pressure) vortex is seen at the position nearly over the sink forcing at the bottom, but the intensity of the vortex is much weaker than that of clockwise vortex forced by a single source at the same rotation rate (Fig. 11 (b)). Such a counterclockwise vortex is more unstable than a clockwise vortex. The difference between the clockwise and the counterclockwise vortices in their strength and stability would be one of the causes of both the predominance of clockwise vortices and the nonsymmetrical frequency distribution of vorticity in multiple forcing experiments.

It should be noted that the flow field created by a single forcing is much different from that created by a multiple forcing. The scale of the vortex in the supplementary experiments with the single forcing is much larger than that in the experiments with the multiple forcing. The velocity distributions in the vertical section show that the two-dimensional velocity field of a vortex generated by the single source forcing is more stable than those generated by multiple source-sink forcing and furthermore extends lower in the tank.

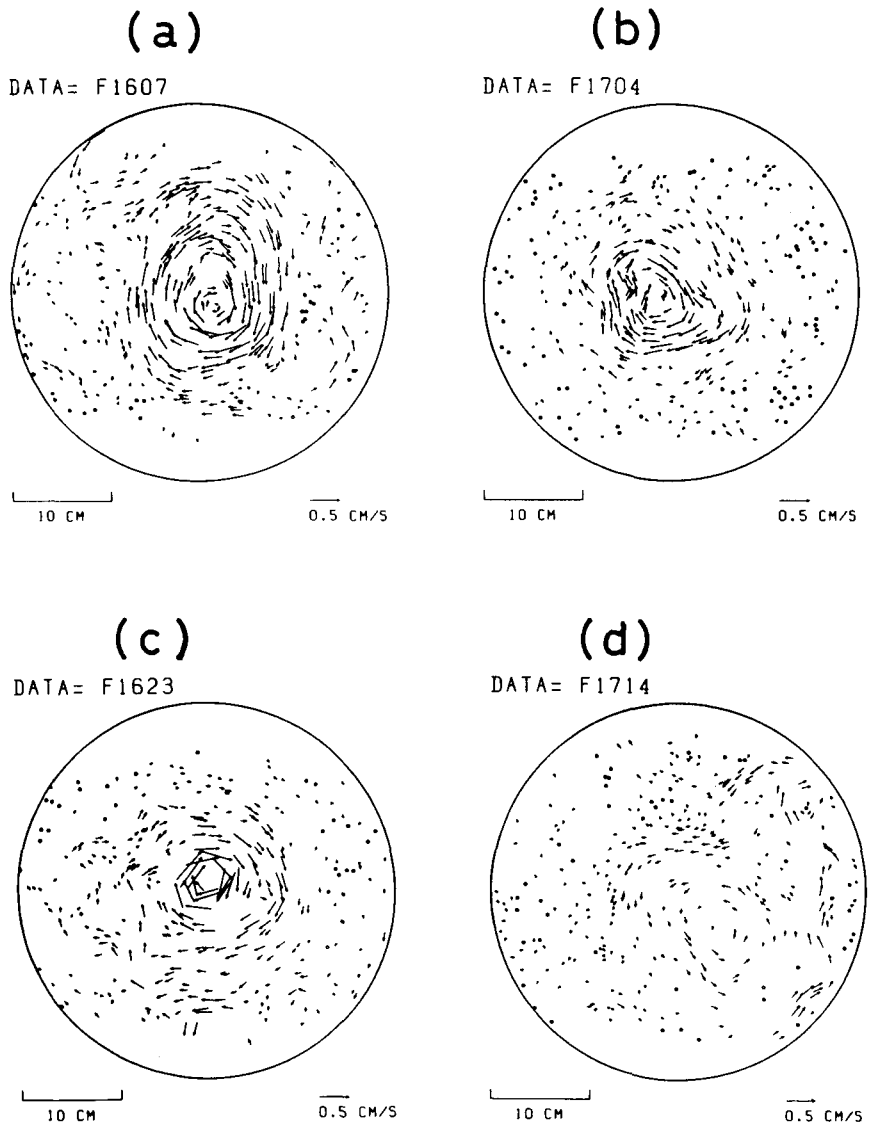

Fig. 11 Examples of visualized velocity field (h=35.5 cm) by a single source or sink forcing in the supplementary experiments. A single source forcing (a) $\Omega=0.43$ rad/s, (b) $\Omega=0.81$ rad/s, (c) $\Omega=1.15$ rad/s. A single sink forcing (d)$\Omega=0.81$ rad/s. For positions of the forcing, the reader should refer to Fig. 3 (a) and 3 (b).

4. Discussions and concluding remarks

The present study investigates the vortex field generated by multiple source-sink forcing in a rotating tank. The flow field in the upper part of the tank consists of many clockwise and counterclockwise vortices which are nearly two-dimensional. The ratio of the number of clockwise (anti-cyclonic) vortices to the total remains a nearly constant 0.7 at any rotation rate. In spite of the predominance of clockwise vortices, the spatial mean of the vorticity also remains nearly zero at any rotation rate. The skewness of the frequency distribution has no clear dependency on the rotation rate either. These facts indicate that some dynamical similarity exists in the redistribution process of vorticity, which is strongly constrained by the law of total vorticity conservation.

The horizontal scale of the vortices can be roughly estimated using the density number of vortics. The mean numbers of the vortices in the flow visualized area are 10.0, 15.6 and 18.3, for the rotation rates 0.43, 0.81 and 1.15 rad/s, respectively (Fig. 8 (b)). The estimated mean diameters of the vortices are 10.2 cm, 8.1 cm and 7.5 cm, respectively for the rotation rates above. These horizontal scales are about twice the distance between source and sink holes at the bottom. The increase in the vortex scale as the rotation rate is decreased indicates that the interaction between the vortices, increasing their coalescence, is stronger at a lower rotation rate. The less stable vortical positions at the lower rotation rate (see Fig. 7 (a)) would be the result of the strong interaction between vortices. Supplementary experiments with a single source forcing show that the scale of a vortex increases as the rotation rate decreases. This fact supports the strong interaction phenomena at the lower rotation rate mentioned above, since a larger vortex would more readily interact with neighbouring vortices when they are in a limited area of the tank.

The predominance of clockwise (anti-cyclonic) vortices in the present experiment differs greatly from the results of MacEwan (1976) and Hopfinger *et al.* (1982). The reason for the difference is not clear but seems to result partly from a difference in experimental conditions. The tank rotation rate Ω in the present experiment (0.43～1.15 rad/s) is smaller than those in MacEwan (1976) (3～11 rad/s) and Hopfinger *et al.* (1982) (0.2 π～π rad/s). The forcing by source-sink flow in the present experiment is weaker than that in MacEwan (1976) and is a different type of forcing than that used in Hopfinger *et al.* (1982). The resulting magnitudes of the velocity U of distinctive vortices in the present study

range from 0.1 cm/s to 0.3 cm/s. This is less than 10% of those seen in the above other two studies, though the resulting scale L is not so different from those in the other studies. The magnitude of the concentrated vorticity of distinctive vortices in the present study is relatively small (less than 20% of the background vorticity 2Ω). Consequently, the Rossby number $U/2\Omega L$ achieved in the present study is of the same order O (10^{-2}) as in the other two studies. However, the Reynolds number UL/ν in the present study, O (10^2), is much smaller than those, O (10^3), obtained in other studies.

The supplementary experiments suggest that the predominance of clockwise vortices in the present study would also be partly due to the source-sink process at the bottom of the present tank system. They show that a clockwise vortex is generated by source forcing and a counterclokwise vortex by sink forcing. The clockwise vortex generated is more intense and distinct than the counterclockwise one. This would be a result of the difference between source forcing and sink forcing. The source forcing is generally thought to be a clearer type of jet flow than the sink forcing.

The flow visualization used in the present study has revealed the detailed velocity distribution of the vortex field in the rotating system. The redistribution process of the vorticity is discussed, based on the velocity field visualization. The present supplementary experiments also reveal that the characteristic features (e.g. size, strength, stability) of vortices generated by a single source or sink are much different from those generated by a multiple source-sink. Further measurements focusing on the behavior of single vortices within the vortex field will be necessary in order to clarify the vortical process, from generation to dissolution, including the interaction process between the vortices. The present flow visualization technique, however, is slow and laborious. In view of the fact that the vortex field is somewhat turbulent, further systematic, continuous measurements with electrical devices (such as a laser anemometer) that yield large amounts of statistical data would be very productive, used in conjunction with the instantaneous visualization techniques utilized in this experiment.

Acknowledgements

We would like to express our great thanks to Mr. M. Okayama of Research Center for Earthquake Prediction, Hokkaido University for his generous help in designing and constructing the programmable electric signal retarder. Thanks are also due to several members of the Department of Geophysics, Hokkaido

University : to Dr. K. Takeuchi for his discussions, to Dr. T. Moriya for his advice on the design of the electric retarder, to Miss H. Hikino for her asistance in preparing the digitized co-ordinate data of flow visualizations, to Misses C. Imai and I. Hisahara for their typing the manuscript. The computer data processing including the preparation of the digitized data was carried out at the Hokkaido University Computing Center. This study was supported by a Grant-in-Aid for Scientific Research from the Ministry of Education, Science and Culture, Project No. 59540234.

References

Bretherton, F.P. and Turner, J.S., 1968. On the mixing of angular momentum in a stirred rotating fluid. J. Fluid Mech., **32** : 449-464.

Colin de Verdiere, A., 1980. Quasi-geostrophic turbulence in a rotating homogeneous fluid. Geophys. Astrophys. Fluid Dyn., **15** : 213-251.

Dickinson, S.C. and Long, R.R., 1983. Oscillating grid turbulence including effects of rotation. J. Fluid Mech., **126** : 315-333.

Gough, D.O. and Lynden-Bell, D., 1968. Vorticity expulsion by turbulence : astrophysical implications of an Alka-Seltzer experiment. J. Fluid Mech., **32** : 437-447.

Hopfinger, E.J., Browand, F.K. and Gagne, Y., 1982. Turbulence and waves in a rotatiog tank. J. Fluid Mech., **125** : 505-534.

Koga, M., 1981. Direct production of droplets from breaking wind-waves : its observation by a multi-colored overlapping exposure photographing technique. Tellus, **33** : 552-563.

Long, R.R., 1956. Sources and sinks at the axis of a rotating liquid. Quart. J. Mech. App. Math., **9** : 385-393.

Long, R.R., 1958. Vortex motion in a viscous fluid. J. Meteor., **15** : 108-112.

McEwan, A.D., 1976. Angular momentum diffusion and the initiation of cyclones. Nature, **260** : 126-128.

Morton, B.R., 1963. Model experiments for vortex columns in the atmosphere. Nature, **197** : 840-842.

Shih, H. and Pao, H., 1971. Selective withdrawal in rotating fluids. J. Fluid Mech., **49** : 509-527.

Tritton, D.J., 1978. Turbulence in rotating fluids, in *Rotating Fluids in Geophysics*, edited by P.H. Roberts and A.M. Soward, pp. 105-138, Academic Press.

Turner, J.S. and Lilly, D.K., 1963. The carbonated-water tornado vortex. J. Atmos. sci., **20** : 468-471.